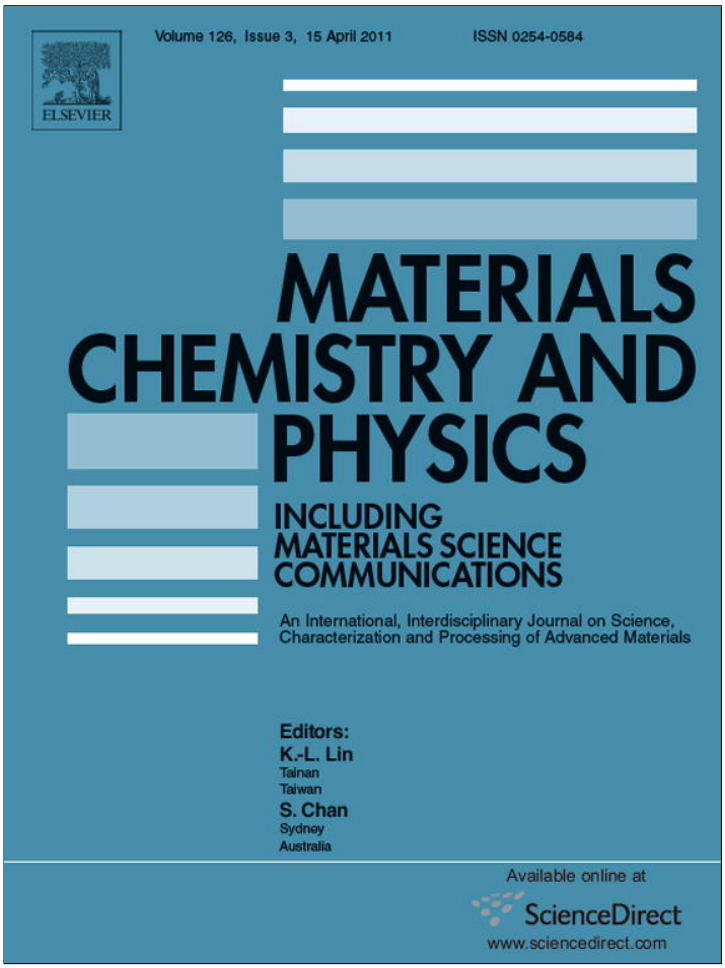

Materials Chemistry and Physics 126 (2011) 938–947

Contents lists available at ScienceDirect

Materials Chemistry and Physics

journal homepage: www.elsevier.com/locate/matchemphys

The incidence of chromium-rich corrosion products on the efficiency of an imidazoline-based inhibitor used for CO_2 corrosion prevention

L.D. Paolinelli[a], T. Pérez[b], S.N. Simison[a,*]

[a] División Corrosión – INTEMA, UNMdP, Ave. Juan B. Justo 4302, B7608FDQ Mar del Plata, Bs. As., Argentina
[b] R&D TENARIS SIDERCA, Simini 250, Campana 2804, Bs. As., Argentina

ARTICLE INFO

Article history:
Received 27 August 2009
Received in revised form
30 November 2010
Accepted 2 December 2010

Keywords:
Corrosion
Microstructure
SEM
EDS

ABSTRACT

A study has been conducted to analyze the influence of 1% Cr additions, microstructure, and pre-corrosion on the performance of CO_2 corrosion inhibitors for C–Mn steels. Two carbon steels with two different microstructures were tested in a deoxygenated 5 wt.% NaCl solution, saturated with CO_2 at 40 °C, pH 6. An imidazoline-based inhibitor was added after different pre-corrosion periods. Its performance was studied by means of d.c. electrochemical measurements, SEM and EDS. The results demonstrated a detrimental effect of 1% Cr and pre-corrosion on the inhibitor efficiency. It was also proven that the impact of pre-corrosion depends on microstructure and chemical composition.

1. Introduction

CO_2 corrosion is an important concern for the oil and gas industry. It is a very complex issue due to the multiple variables involved: environmental (CO_2 concentration, temperature, pH, among others), physical (flow condition, water wetting, etc.) and metallurgical (chemical composition and microstructure of steel) [1–3].

In relation to the influence of chemical composition and microstructure of carbon and low alloy steel on CO_2 corrosion, contradictory results can be found in the literature [4,5], besides no general mechanism has been established yet. Particularly the effect of those variables on the corrosion product film formation and on the inhibitor performance remains to be fully understood.

A positive contribution of low Cr additions (up to 5%) to the corrosion resistance of standard carbon steel has been reported [5–12]. In environments with a moderate CO_2 content, a combination of an addition of 3% Cr, a correct microalloying and heat treatment can improve corrosion resistance of low alloy steels, based on the formation of a stable protective chromium containing oxide film [9–11]. However, Kermani et al. [5,12] stated that Cr is effective only above a given level; if below, it could be detrimental to the anodic reaction on bare steel (1–1.5% Cr at pH 5.3).

Little is known about the role that chemical composition of carbon steel plays on the efficiency of inhibitors and/or on the protective film formation. In particular, a detrimental effect of Cr has been reported for low Cr alloyed steels (0.5–1%) [13–16]; yet no explanation has been given.

Even though SAE 1018 constitutes the most common substrate used for inhibitor performance tests, some articles in literature account for considerable differences in the efficiency of individual inhibitors on different steels [17,18].

Irrespective of the protection mechanism of a given inhibitor, to achieve a satisfactory performance, the inhibitor should interact with the surface to be protected. Therefore, it could be anticipated that its efficiency should be affected by the nature and morphology of corrosion products. The efficiency of inhibitors should then be conditioned by chemical composition and microstructure of steel as well as by the previous extent of corrosion.

Former works have reported that the efficiency of inhibitors for C–Mn steels is influenced by microstructure and that such influence could be specific to the inhibitor molecular structure [19–22].

It has also been demonstrated that pre-corrosion has a negative effect on inhibitor efficiency and that this effect is dependent on microstructure [23]. Other authors have also discussed the importance of pre-corrosion on inhibitor efficiency [17,24,25].

More recently, it has been shown that the addition of 1% Cr has a notorious detrimental effect on the performance of a commercial imidazoline-based inhibitor when samples are pre-corroded for 72 h [26].

This work aims at exploring the influence of 1% chromium content and microstructure of a C–Mn steel as well as pre-corrosion conditions on the efficiency of a commercial inhibitor in CO_2 corrosion.

* Corresponding author. Tel.: +54 223 4816600x244; fax: +54 223 4810046.
E-mail address: ssimison@fi.mdp.edu.ar (S.N. Simison).

0254-0584/$ – see front matter © 2010 Elsevier B.V. All rights reserved.
doi:10.1016/j.matchemphys.2010.12.001

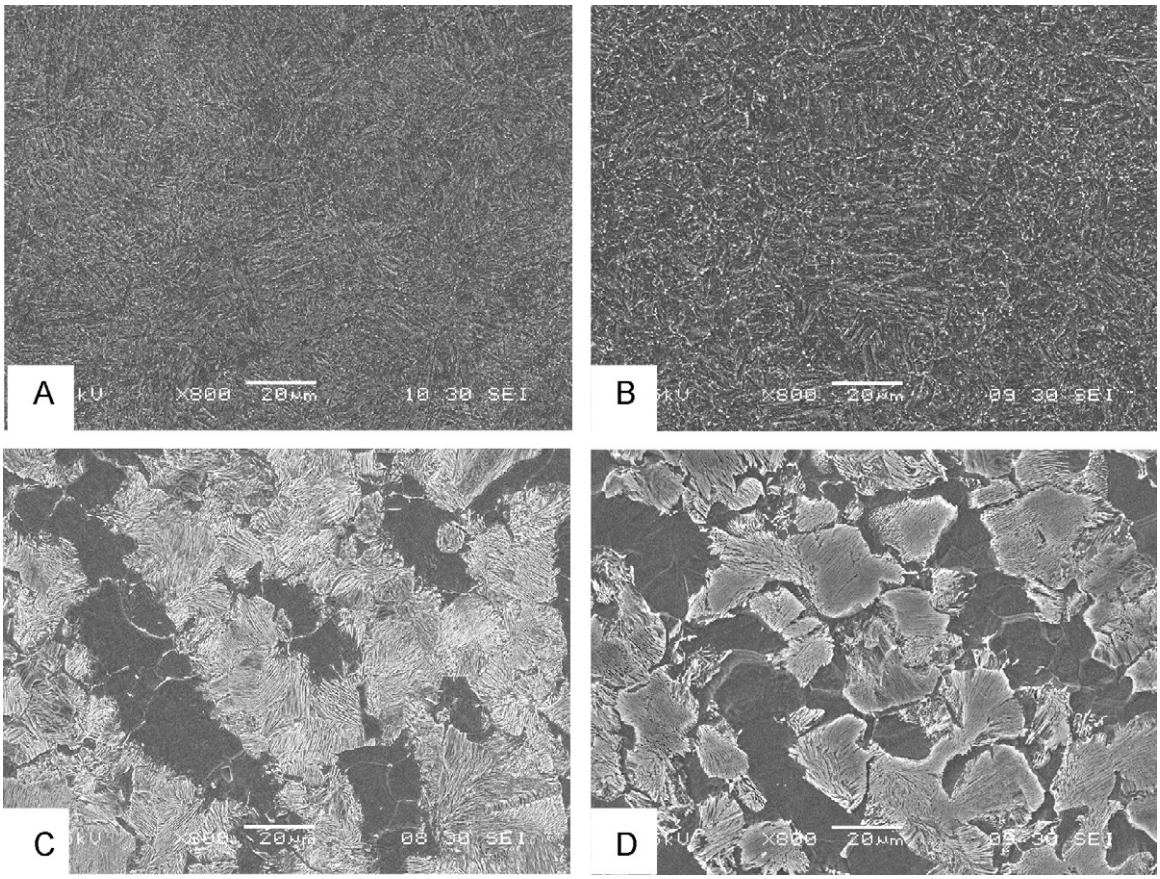

Fig. 1. Microstructural features: (A) TM–1Cr, (B) TM–C–Mn, (C) FP–1Cr and (D) FP–C–Mn.

2. Materials and methods

A steel with the following composition (wt.%): 0.39 C–1.01 Mn–0.26 Si–1.02 Cr (named 1Cr) was used. Two different heat treatments: annealing and quenching-tempering were conducted on the material in a lab furnace. The annealing treatment comprised an austenitization at 890 °C and cooling inside the furnace (FP sample). The quenching and tempering treatment (Q&T), in turn, consisted of an austenitization at 890 °C, followed by water quenching and a tempering treatment at 700 °C for 1 h (TM sample). Heat treatment conditions were selected to obtain two distinctive cementite morphologies (coarse laminar and globular).

To evaluate the effect of 1% Cr content, the results were compared with those obtained from a carbon steel with the following composition (wt.%): 0.38 C–0.99 Mn–0.33 Si–0.17 Cr (named C–Mn), and with the same heat treatments [23]. Fig. 1 illustrates the microstructural characteristics of both steels.

Working electrodes were obtained from these heat-treated materials by machining 5 mm diameter bars, cut and mounted with epoxy resin on plastic holders. The electrical contact between the sample and the holder was obtained with silver-loaded epoxy resin. The surfaces exposed were abraded with 600-grit SiC paper, washed with distilled water, rinsed with ethanol, and dried with a cool air current.

Experiments were conducted at atmospheric pressure, 40 °C and low speed magnetic stirring (100 rpm). Three-electrode jacketed test cells with a working volume of 0.5 L were employed and a concentric Pt ring was used as a counter electrode. A saturated calomel electrode (SCE) was chosen as reference. The test solution was 5 wt.% NaCl (analytical-reagent grade), saturated with deoxygenated CO_2. The oxygen concentration of the solution was measured with a Fibox 3-trace v3 PreSens® and kept below 4×10^{-2} ppm during the experiments. To avoid the presence of air, a positive pressure of deoxygenated CO_2 was maintained throughout the tests. The pH was adjusted to 6 by adding deoxygenated 1.0 mol L^{-1} $NaHCO_3$ solution.

A commercial imidazoline-based product ($R_1 = (CH_2)_n–CH_3$ $n = 10–17$, $R_2 = (CH_2)_2–NH_2$) was used as inhibitor (Fig. 2). Following the inhibitor manufacturer specifications, a concentration of 50 ppm was employed.

A Voltalab® PGZ 402 unit was utilized for the electrochemical measurements. Linear polarization resistance (LPR) was measured by polarizing the working electrode ±15 mV vs. the corrosion potential (Ecorr) with a sweep rate of 0.1 mV s^{-1}. The corrosion potential was also monitored before and after the d.c. analyses. All the electrochemical results are average values from at least eight replicas of each experimental condition.

Corrosion rates (CR) were calculated from polarization resistance (Rp) values by means of the Stern Geary equation with a proportionality factor $B = 0.022$ V [27].

The inhibitor was added at the beginning of the experiments (with no pre-corrosion) and after pre-corrosion periods of 24 and 72 h. The formation of the inhibitor film was evaluated at the first 2 h and then every 24 h for 3 days.

A scanning electron microscope (SEM Phillips® XL 30) equipped with EDS was used for surface film characterization. Image analysis was performed by means of Image Pro Plus® software.

3. Results

3.1. Corrosion potentials and linear polarization resistance

Table 1 lists the results of d.c. tests performed on steel samples of both chemical compositions and microstructures. Ecorr and corrosion rate (CR) values obtained after different corrosion periods are also shown therein. Corrosion rates are higher for chromium containing steel, this effect being especially significant for the ferritic–pearlitic microstructure. No significant changes in corrosion potentials are reported.

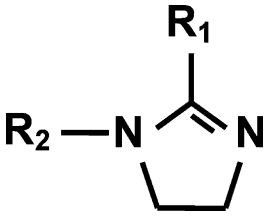

Fig. 2. Schematic representation of an Imidazoline molecule.

Table 1
Ecorr and CR values vs. time for the different steels and microstructures exposed to non-inhibited solution.

Exposure (h)	TM				FP			
	1Cr		C–Mn		1Cr		C–Mn	
	Ecorr (mV/SCE)	CR (mm y^{-1})	Ecorr (mV/SCE)	CR (mm y^{-1})	Ecorr (mV/SCE)	CR (mm y^{-1})	Ecorr (mV/SCE)	CR (mm y^{-1})
24	−747	1.60 ± 0.11	−749	1.49 ± 0.12	−741	1.9 ± 0.09	−747	1.47 ± 0.15
48	−742	1.85 ± 0.1	−745	1.54 ± 0.17	−733	2.21 ± 0.17	−743	1.35 ± 0.14
72	−738	2.05 ± 0.12	−743	1.67 ± 0.25	−727	2.49 ± 0.23	−739	1.33 ± 0.19

Table 2
Ecorr and CR values vs. time for the different steels and microstructures exposed to the inhibited solution without pre-corrosion.

Exposure (h)	TM				FP			
	1Cr		C–Mn		1Cr		C–Mn	
	Ecorr (mV/SCE)	CR (μm y^{-1})	Ecorr (mV/SCE)	CR (μm y^{-1})	Ecorr (mV/SCE)	CR (μm y^{-1})	Ecorr (mV/SCE)	CR (μm y^{-1})
2	−682	70 ± 21	−650	17.4 ± 1.3	−697	206 ± 50	−659	20.6 ± 3.9
24	−690	33 ± 8	−649	5.8 ± 1	−709	144 ± 46	−646	6.4 ± 0.1
48	−699	28 ± 4	−650	4.5 ± 0.6	−715	134 ± 41	−643	5.8 ± 0.9
72	−704	26 ± 3	−656	4.5 ± 1	−717	138 ± 48	−649	5.8 ± 0.6

Table 3
Ecorr and CR values vs. time for the different steels and microstructures with 24 h of pre-corrosion exposed to the inhibited solution.

Exposure (h)	TM				FP			
	1Cr		C–Mn		1Cr		C–Mn	
	Ecorr (mV/SCE)	CR (μm y^{-1})	Ecorr (mV/SCE)	CR (μm y^{-1})	Ecorr (mV/SCE)	CR (μm y^{-1})	Ecorr (mV/SCE)	CR (μm y^{-1})
2	−706	582 ± 150	−665	90 ± 29	−688	605 ± 144	−671	177 ± 27
24	−701	195 ± 52	−638	13 ± 3	−693	450 ± 108	−628	21 ± 4
48	−707	139 ± 43	−622	12 ± 3	−698	423 ± 112	−634	15 ± 1
72	−709	110 ± 34	−634	9 ± 3	−700	412 ± 125	−623	14 ± 4

Table 4
Ecorr and CR vs. time for the different steels and microstructures with 72 h of pre-corrosion exposed to the inhibited solution.

Exposure (h)	TM				FP			
	1Cr		C–Mn		1Cr		C–Mn	
	Ecorr (mV/SCE)	CR (μm y^{-1})	Ecorr (mV/SCE)	CR (μm y^{-1})	Ecorr (mV/SCE)	CR (μm y^{-1})	Ecorr (mV/SCE)	CR (μm y^{-1})
2	−718	1445 ± 258	−689	292 ± 131	−709	1677 ± 193	−698	240 ± 88
24	−703	606 ± 103	−639	23 ± 6	−686	877 ± 181	−648	23 ± 5
48	−707	439 ± 129	−625	19 ± 5	−694	929 ± 258	−643	18 ± 3
72	−710	361 ± 129	−626	15 ± 5	−696	955 ± 297	−644	18 ± 3

Tables 2–4 illustrate the effect of the inhibitor addition on fresh (non-pre-corroded) and pre-corroded samples. Indeed, the corrosion rate decreases with inhibition time; yet the negative effect of Cr addition is notorious.

When comparing Tables 1–4, it can be seen that the inhibitor addition shifts the corrosion potential to more positive values for all the experimental conditions. According to the literature [27–30], this fact denotes the anodic character of the inhibitor employed in this study. Previous work [23] using polarization curves has shown that this inhibitor reduces both cathodic and anodic reactions. As the change in the last reaction is more significant, the corrosion potential shifts in the positive direction.

It is worth noting that the corrosion rate reduction resulting from the inhibitor addition depends on the steel microstructure, the length of the inhibition period, and mainly on the chemical composition of steel. The detrimental effect of pre-corrosion, particularly for 1Cr steel, is also clear.

With respect to microstructure, it can be observed that for both steels, TM samples behave better under most of the evaluated conditions, especially for 1Cr steel.

Inhibitor efficiencies were calculated by applying Eq. (1). The values obtained for 1Cr steel are presented in Table 5. Efficiencies for C–Mn steel have not been included as they all approach 100% before 48 h of inhibition, even for the longest pre-corrosion period tested (72 h) [23].

$$\eta = \left(1 - \frac{\mathrm{Rp}}{\mathrm{Rp'}}\right) 100 \quad (1)$$

where η: inhibitor efficiency (%), Rp: polarization resistance value measured without the inhibitor, Rp′: polarization resistance value measured with the inhibitor added.

Table 5
Inhibitor efficiency (%) vs. time for 1Cr steel samples with different microstructures and pre-corrosion periods.

Exposure (h)	TM			FP		
	Pre-corrosion period (h)			Pre-corrosion period (h)		
	0	24	72	0	24	72
2	96	64	29	88	68	31
24	98	88	70	92	76	64
48	98	91	78	93	78	62
72	98	93	82	92	78	61

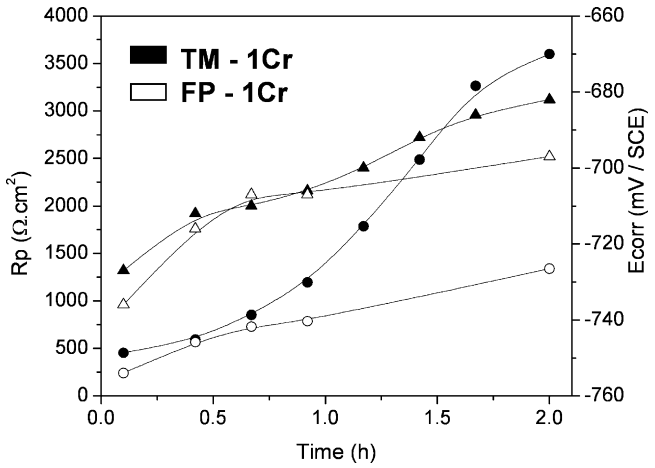

Fig. 3. Polarization resistance (○) and Ecorr (Δ) vs. time for inhibited 1Cr steel fresh samples.

It can be seen that the inhibitor efficiency tends to improve with exposure time except for ferritic–pearlitic samples, particularly pre-corroded ones.

With a view to understanding the disparity in inhibitor efficiency between the two microstructures for 1Cr steel, some short duration experiments were performed on fresh samples. LPR measurements were carried out during the first 2 h of immersion. These measurements can be used to understand the kinetics of the inhibitor adsorption since, for short exposures, the increase of Rp values is directly related to the surface coverage. Fig. 3 demonstrates that the inhibitor coverage is faster and better on TM samples.

3.2. Surface analysis

SEM images of corroded samples are shown in Figs. 4–8.

No significant differences can be appreciated in surface morphology between both steels without inhibitor addition (Fig. 4). The attack is uniform over the whole surface exposed. Regarding microstructure, TM samples exhibit a corrosion product layer, which has embedded globular carbides only detectable at high magnification (Fig. 4A–D). As to the ferritic–pearlitic microstructure, a common corrosion pattern can be observed for both steels; ferrite corrodes preferentially (Fig. 4E–H). Consequently, the steel microstructure is revealed and a corrosion product film is formed on the pearlite colonies. At high magnification, a surface product can also be noticed on top of the ferrite grains of 1Cr steel (Fig. 4G). This product is absent in C–Mn steel (Fig. 4H).

The chromium content of 1Cr steel corrosion products measured by EDS is shown in Table 6. Results indicate an enrichment of this element throughout the time of exposure to non-inhibited solution. For example, after 24 h, corrosion products yield an average Cr content of 3.5% on both microstructures. However, for ferritic–pearlitic samples Cr content is not homogeneous throughout the whole surface as it is the case for TM samples. The average Cr content values are 2 and 4% on ferrite and pearlite, respectively. As already mentioned, Cr content is 3.5% when a larger region, including several ferrite grains and pearlite colonies, is analyzed.

Table 6
Surface chromium content (wt.%, EDS) vs. time for 1Cr steel samples with different microstructures exposed to non-inhibited solution.

Exposure (h)	TM	FP		
	General	General	Ferrite	Pearlite
0 (uncorroded)	1.1	1.2	1.2	1.2
4	1.6	1.6	1.6	1.6
24	3.5	3.5	2	4
72	8	8	4	9

When the samples, either pre-corroded or not, are placed in contact with the inhibited solution, the attack morphologies obtained are significantly different for both steels (Figs. 5 and 6). C–Mn steel continues presenting generalized corrosion, while for 1Cr steel attack becomes localized. The severity of the localized attack of 1Cr steel is dependent on microstructure as well as on pre-corrosion period.

After 24 h of pre-corrosion and 72 h of inhibition, C–Mn steel corroded surfaces mirror those found without the inhibitor addition (Fig. 5B and D). Due to the high effectiveness of the inhibitor, only a slight increase in the amount of corrosion products can be detected on the surface (Fig. 5F). For both 1Cr steel microstructures, two distinctive patterns are observed. On the one hand, most of the surface displays the same morphology as that found at the end of the pre-corrosion period (before inhibitor addition). On the other hand, localized zones with thick corrosion products that seem to cover deep attacked areas are also detected (Fig. 5A, C and E). These different patterns would indicate that the inhibitor is effective in reducing the corrosion rate on most of the specimen surface, yet leaving zones where corrosion keeps on acting.

Similar surface morphology patterns are found in 1Cr steel samples with 72 h of pre-corrosion and 72 h of inhibition.

Fresh samples immersed in the inhibited solution during 72 h also exhibit the patterns described above (Fig. 6). C–Mn steel shows a slight attack in part of its surface that could have occurred before the complete inhibitor film coverage (Fig. 6B, D, F and H). With respect to 1Cr steel, most of the surface remains unattacked, while there are fractions of the surface where the attack seems to be even more localized than in the pre-corroded condition described above (Fig. 6A, C, E and G).

In the case of 1Cr steel samples pre-corroded for 24 and 72 h and with 72 h of inhibition, Cr content is kept practically constant in the zones where the inhibitor is efficient while enrichments of up to 13 and 16% can be found in the localized attack zones for TM and FP microstructures, respectively (Table 7). Inhibited fresh samples also yield high Cr contents in the corrosion products where localized attack occurred, while they are similar to the blank in the rest of the surface.

As a way to determine when the localized corrosion areas could have been produced during the 72 h of inhibition, 1Cr steel surfaces were observed after 4 and 24 h of inhibition (Figs. 7 and 8, respectively).

As it can be seen, even for short exposure periods (Fig. 7), there are areas where the inhibitor does not act. This is consistent with the increase of Cr content found in the affected areas (Table 7, no pre-corrosion and 4 h of inhibition), considering that the average Cr content on non-inhibited samples corroded for 4 h was 1.6% on the whole surface (Table 6). After 24 h of inhibition, the only visible change is that the attack has concentrated in those areas originally affected (Fig. 8).

Transversal cuts were performed on some samples at the end of long duration experiments (72 h of inhibition) to evaluate the final depth of the attack (Fig. 9). For both steels corroded without inhibitor addition, the attack was generalized and homogeneous throughout the entire section. The same was determined for C–Mn steel after 72 h of inhibition regardless of the pre-corrosion period [23].

In the case of FP–1Cr inhibited samples, the attack is irregular, yielding a higher metal loss in non-inhibited zones where remaining uncorroded cementite lamellae can be clearly observed (Fig. 9A and C). For the same experimental condition, the attack in TM–1Cr samples (Fig. 9B and D) is more localized and deeper than in FP–1Cr

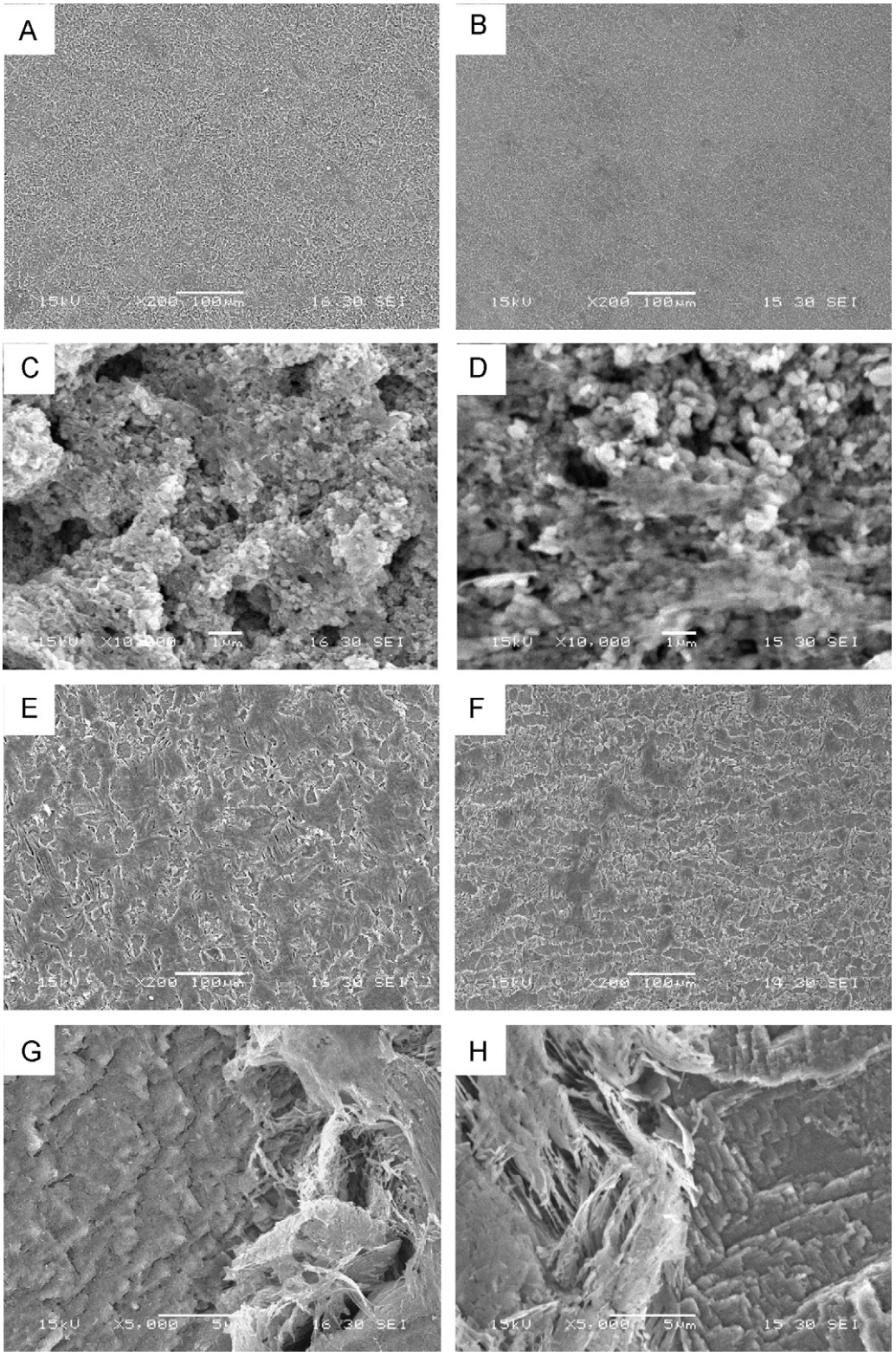

Fig. 4. Surface morphology of steel samples pre-corroded for 24 h. General view: (A) TM–1Cr, (B) TM–C–Mn, (E) FP–1Cr and (F) FP–C–Mn. High magnification view: (C) TM–1Cr, (D) TM–C–Mn, (G) FP–1Cr and (H) FP–C–Mn.

ones. Additionally, the corrosion products are thicker within the affected zone (Fig. 9D).

To estimate the fraction of area affected by localized corrosion (Table 8) SEM images of the inhibited 1Cr steel samples were analyzed by software, differentiating the attacked zones from the protected ones and quantifying the projected areas of damage. Indeed, the fraction of affected surface is shown as an interval, because of the random nature of the localized corrosion. Yet, a clear difference between microstructures exists since the attack is less localized for ferritic–pearlitic one.

After 72 h of inhibition, unprotected zones of non-pre-corroded 1Cr steel samples present maximum depths of 50

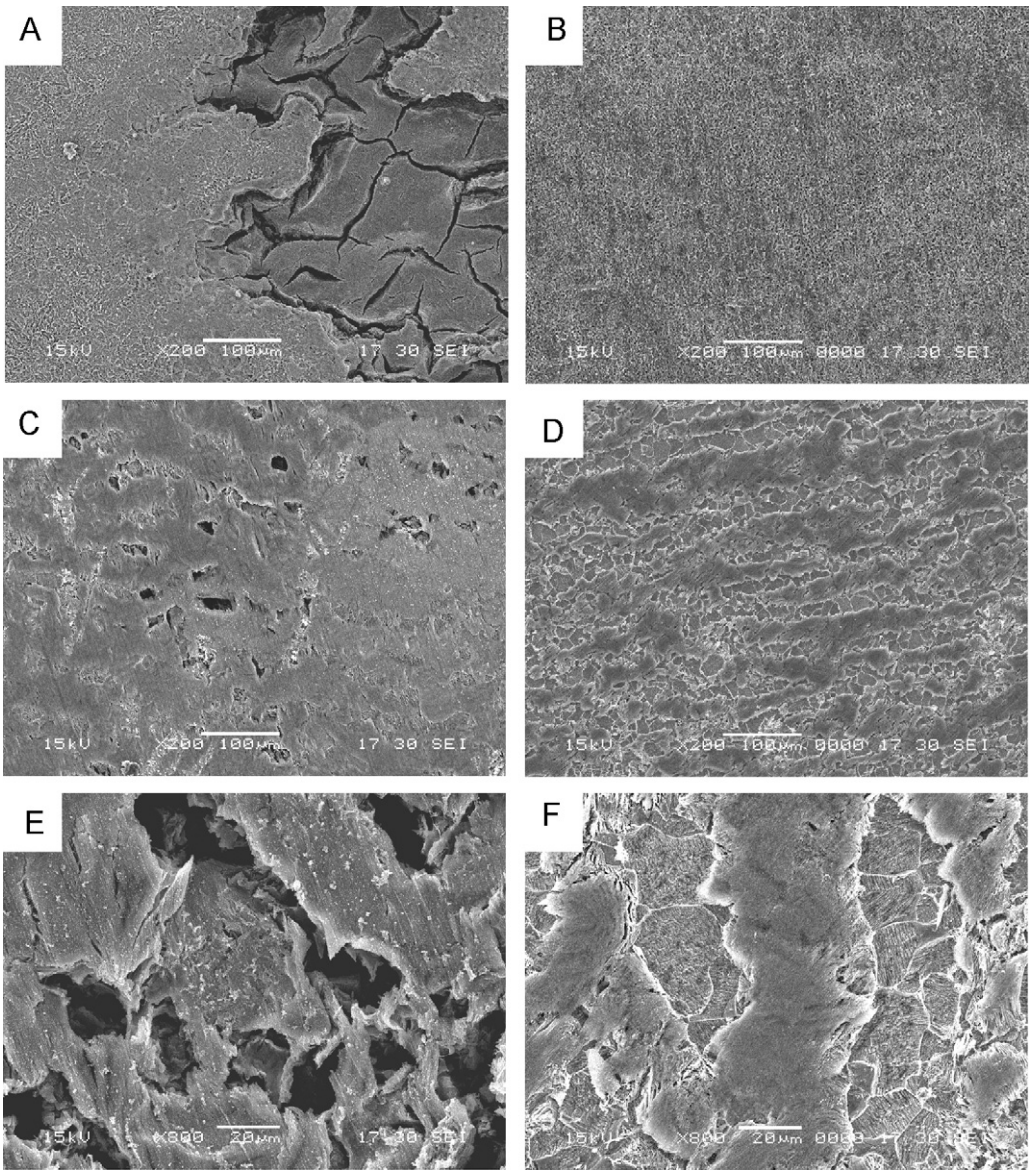

Fig. 5. Surface morphology of steel samples pre-corroded for 24 h and inhibited for 72 h. General view: (A) TM–1Cr, (B) TM–C–Mn, (C) FP–1Cr and (D) FP–C–Mn. High magnification view: (E) FP–1Cr and (F) FP–C–Mn.

Table 7
Surface chromium content (wt.%, EDS) vs. pre-corrosion time for 1Cr steel samples with different microstructures inhibited for 72 h. (NA): non-attacked. (—) Non-resolved (heavily covered by corrosion products).

Pre-corrosion (h)	TM		FP					
	Inhibited	Attacked	Inhibited			Attacked		
			General	Ferrite	Pearlite	General	Ferrite	Pearlite
0[a]	1.4	3	1.4	NA	NA	2.5	2	3
0	1.5	13	1.4	NA	NA	10	11	10
24	3.5	13	4	2	4	16	–	–
72	7	11.5	8.5	3.5	9	16	–	–

[a] 4 h of inhibition.

and 85 μm (Table 8), that lead to average corrosion rates of 6 and 10 mm y^{-1} for FP and TM microstructures, respectively. In the case of samples pre-corroded for 72 h, the measured depths are 75 and 55 μm, yielding average corrosion rates of 9 and 6.7 mm y^{-1} for FP and TM microstructures, respectively. Regardless of the tested microstructure or pre-corrosion period, the estimated corrosion rates in unprotected zones are at least 3 times greater than those measured in the absence of inhibitor.

4. Discussion

The increase in corrosion rate of steel with immersion time in non-inhibited solutions (Table 1) could be attributed to the

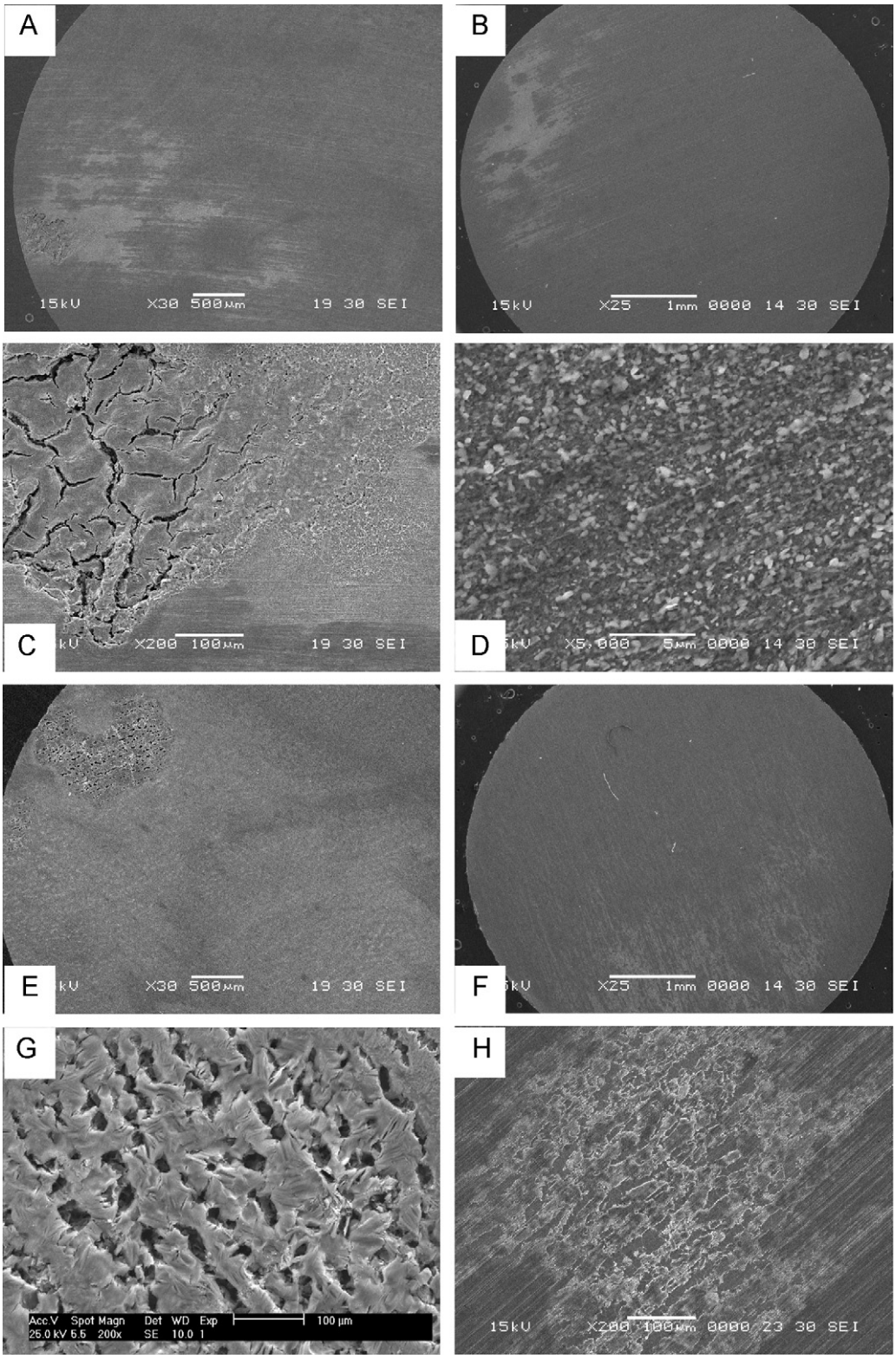

Fig. 6. Surface morphology of fresh steel samples inhibited for 72 h. General view: (A) TM–1Cr, (B) TM–C–Mn, (E) FP–1Cr and (F) FP–C–Mn. High magnification view: (C) TM–1Cr, (D) TM–C–Mn, (G) FP–1Cr and (H) FP–C–Mn.

accumulation of iron carbide particles on the corroded surfaces. Uncorroded cementite provides an available area for the cathodic reactions [31] and, thus, increases corrosion rate of steel. Consequently, corrosion rate is expected to be higher for ferritic–pearlitic microstructure since lamellar cementite has the higher surface/volume ratio and the more favourable shape and size to remain attached to the steel surface after the ferrite dissolution.

However, the present results reveal that the corrosion rate slightly decreases with time for C–Mn FP samples. This particu-

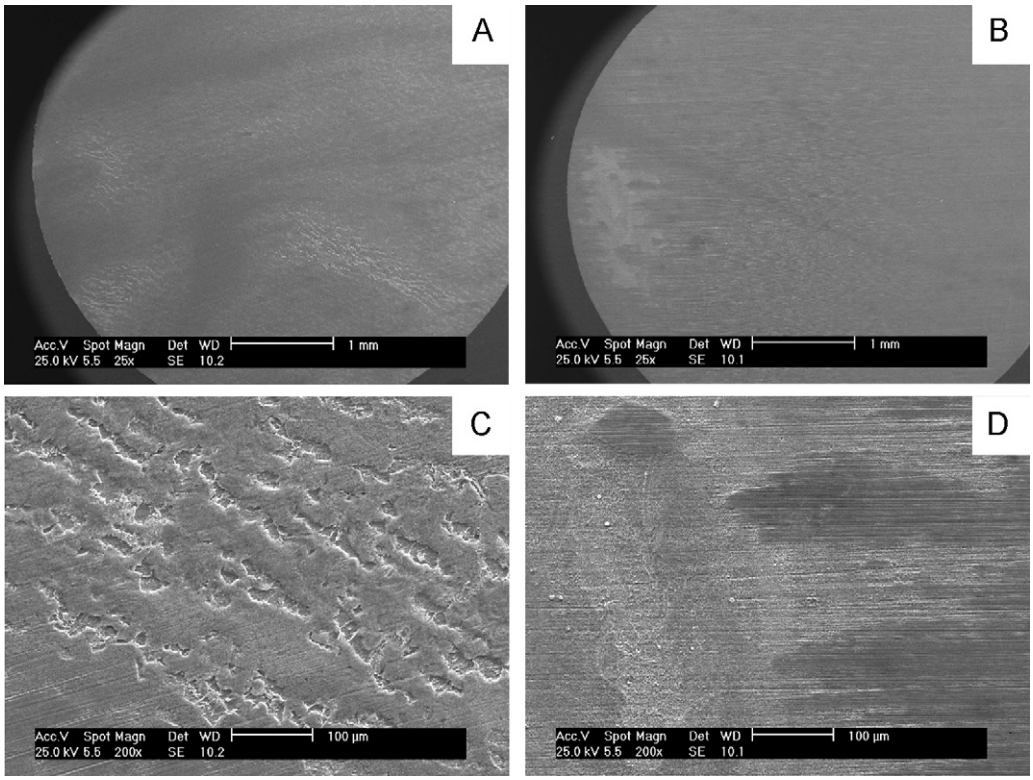

Fig. 7. Surface morphology of 1Cr steel fresh samples inhibited for 4 h. General view: (A) FP–1Cr and (B) TM–1Cr. High magnification view: (C) FP–1Cr and (D) TM–1Cr.

lar effect may be connected to the presence of a partially covering $FeCO_3$ protective film [19,20], that precipitates favoured by the increase in ferrous ion concentration within the cementite lamellae in the former pearlite colonies. It has been proposed [32,33] that the exposed lamellae also have an anchoring effect that contributes to the film stability.

The higher corrosion rates measured on 1Cr steel could be ascribed to presence of chromium-rich corrosion products that

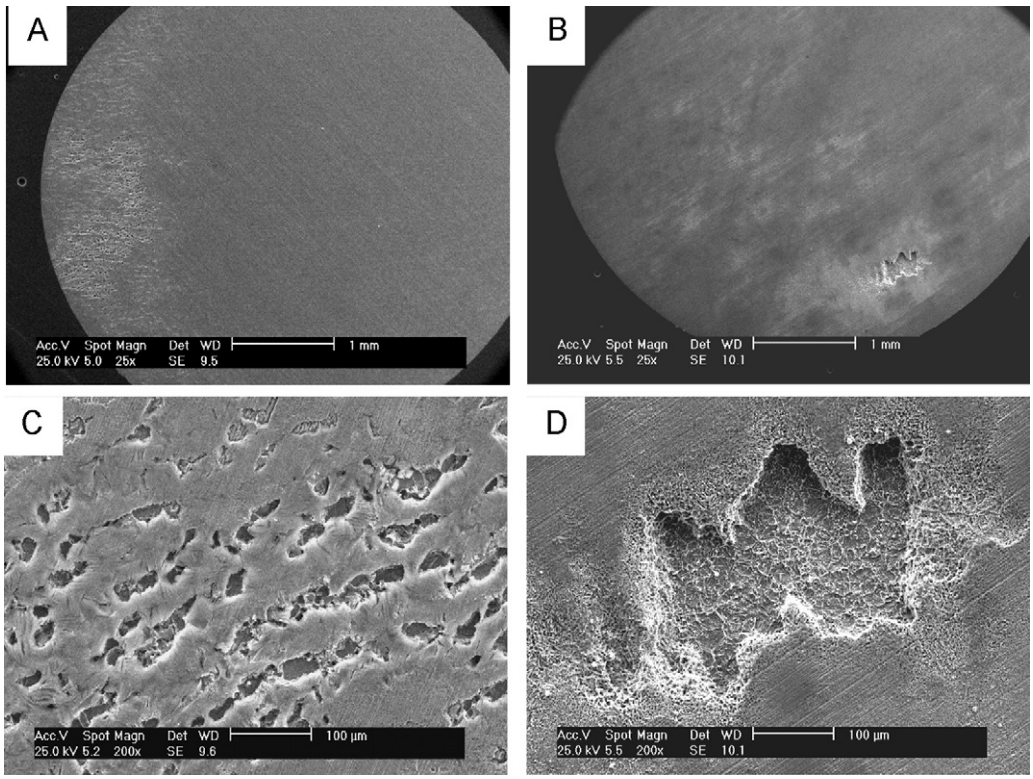

Fig. 8. Surface morphology of 1Cr steel fresh samples inhibited for 24 h. General view: (A) FP–1Cr and (B) TM–1Cr. High magnification view: (C) FP–1Cr and (D) TM–1Cr.

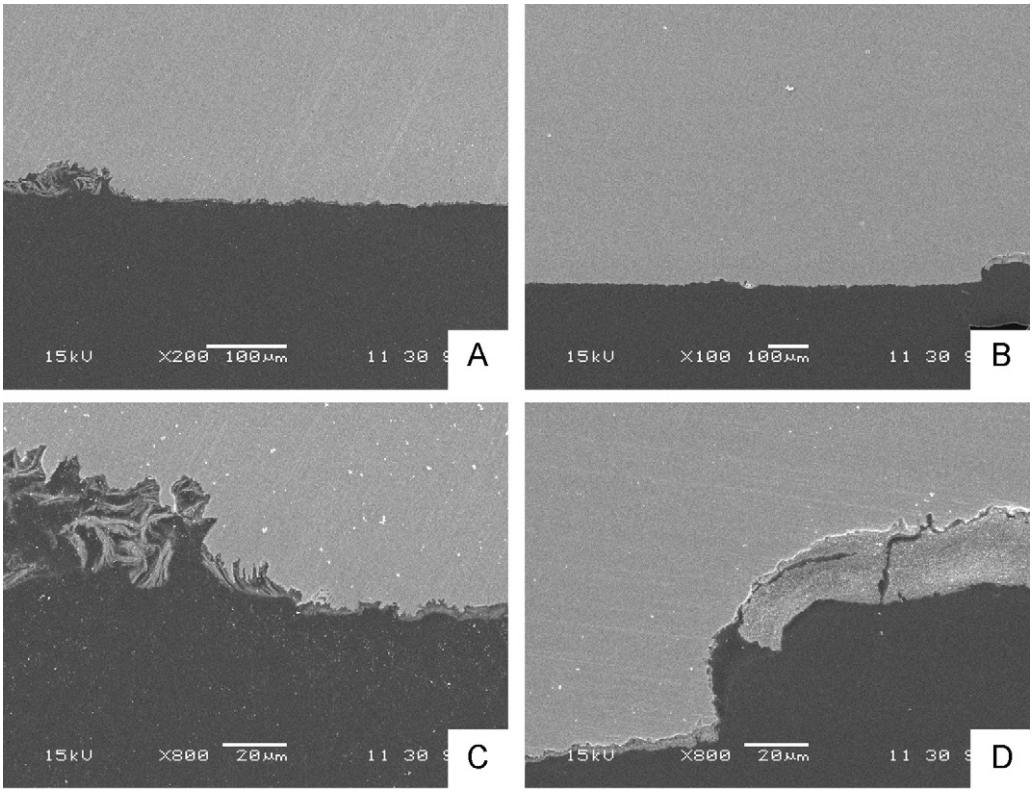

Fig. 9. Localized attack profile (transversal cuts) of 1Cr steel samples pre-corroded for 24 h and inhibited for 72 h. General view: (A) FP–1Cr and (B) TM–1Cr. High magnification view: (C) FP–1Cr and (D) TM–1Cr.

may hamper $FeCO_3$ deposition in the tested conditions. Nose et al. [34] showed that a small amount of Cr (0.6%) in carbon steel was not effective in CO_2 deoxygenated environment where $FeCO_3$ film was formed regardless of Cr content. These authors particularly stated that 0.6% Cr addition seemed to make the $FeCO_3$ film less protective.

When the inhibitor is added to the corrosive solution, an important difference between both steels can be observed.

As opposed to the performance on 1Cr steel, the commercial inhibitor used in this study has proven to be very effective on C–Mn steel even for samples pre-corroded for 72 h (efficiencies higher than 90%). In addition, no significant differences in the inhibitor efficiencies were detected between tempered martensite and ferritic–pearlitic microstructures [23].

Having studied two steels with different chemical compositions and the same microstructure under constant experimental conditions, it is clear that the presence of chromium-rich compounds hinders the adsorption of this imidazoline-based inhibitor on fresh and pre-corroded surfaces. Moreover, from the experiments conducted, it can be deduced that α-Fe containing 1% Cr is a worse substrate for the inhibitor adsorption than Cr-free α-Fe.

Table 8
Fraction of unprotected surface (α) and maximum depth of the localized attack (d) vs. pre-corrosion time for 1Cr steel samples with different microstructures inhibited for 72 h.

Pre-corrosion (h)	TM		FP	
	α (%)	d (μm)	α (%)	d (μm)
0	0.1–1	85	6–10	50
24	1–2.5	85	>10	60
72	5–25	55	>10	75

Regarding the microstructure, the inhibitor adsorbs easier on fresh surfaces of TM–1Cr samples than FP–1Cr ones (Fig. 3). This effect may be linked to their uniform microstructure that consists of an alloyed Fe matrix with a homogeneous distribution of fine carbides. Although it is known that cathodic reactions on cementite are poorly inhibited in CO_2 corrosion [17,18,23], it was proposed elsewhere [22] that imidazoline molecules can be bounded to Fe_3C through Lewis acid–base interactions. Therefore, as chromium alloyed Fe matrix is a deficient substrate for inhibitor adsorption, disperse exposed carbides may act as anchor sites, assisting in the inhibitor film formation and improving film properties and coverage.

Due to the fabrication process FP–1Cr samples have a banded microstructure with strings of ferrite grains and pearlite colonies. In agreement with the analysis applied to TM–1Cr samples, the inhibitor film formation should be better on pearlite, but as alloyed ferrite is poorly protected, the overall film properties and its coverage are worse than in TM–1Cr samples.

As the inhibitor is mainly anodic, it blocks the anodic areas more efficiently. Consequently, as coverage increases, the relationship between anodic and cathodic areas decreases, and so the corrosion rate on the uncovered zones rises (as well as the chromium local concentration in corrosion products). This results in corrosion rates higher than those found in the absence of the inhibitor. Once the chromium concentration of uncovered zones increases, the adsorption of the inhibitor becomes more difficult thereby preventing total area coverage and promoting the progress of localized corrosion. This is particularly critical for TM–1Cr fresh samples due to the faster adsorption rate on them and the corresponding higher coverage degree (Fig. 3).

When 1Cr steel samples are pre-corroded, there is an increment of chromium-rich compounds as well as of iron compounds including uncorroded cementite in corrosion products. As was stated above, the increment of chromium-rich products hinders

the inhibitor adsorption. Consequently, the resulting inhibitor film tends to be more defective and to form more slowly than on fresh surfaces.

From the electrochemical tests, a detrimental effect of pre-corrosion on the inhibition of 1Cr steel may be inferred, but this is not necessarily true since corrosion is not uniform on the whole electrode surface. As already mentioned, the depth of the localized attack of incompletely inhibited samples is determined by the relative anodic and cathodic areas. Hence, the loss of protective inhibitor film quality and coverage with pre-corrosion degree may decrease the actual corrosion rate of affected zones as in the case of TM–1Cr samples (Table 8), turning the attack less localized and then less harmful.

The higher depths of localized attack with pre-corrosion time of inhibited FP–1Cr samples may be tied to the more unfavourable nature of their pre-corroded surfaces. The non-inhibited FP–1Cr samples present greater accumulation of uncorroded cementite along the exposure time than TM–1Cr samples. Then, when the inhibitor is added, the large cementite cathodic areas lead to a decrease in the anodic/cathodic area ratio and so to an increase in the corrosion rate of unprotected zones.

Previous works using XPS identified iron carbonate and cementite as the main corrosion products on C–Mn steels for both microstructures [19,20]. Even though there are no XPS results available at present for the chromium containing steel, the presence of amorphous $Cr(OH)_3$ in the corrosion products of a Q&T 1% Cr steel has been reported [35]. Most likely, this amorphous oxyhydroxide could be the chromium-rich deposit observed on the surfaces of the samples under study.

It must be taken into account that the results describe the performance of this type of inhibitor under simplified experimental conditions and a constricted time window. For these reasons, it is difficult to predict if 1% Cr steels will suffer localized corrosion in service and if this form of corrosion will progress at similar rates than the ones found in this study. In any case, this information represents a warning and emphasizes the importance of employing the same chemical composition and microstructure of steel to be used in service when performing inhibitor selection tests.

In view of the relevance and complexity of this issue, further research should be conducted to address the characterization of the inhibition of Cr alloyed steels in CO_2 media. It could also prove interesting to carry out tests with other inhibitor concentrations so as to determine if localized corrosion could be prevented.

5. Conclusions

The tested inhibitor (a commercial imidazoline-based product) presents very good efficiency on C–Mn steel samples with both ferritic–pearlitic and tempered martensite microstructures. This is explained by the presence of a protective film over the whole exposed area, even when surfaces are pre-corroded.

Low Cr addition (1%) has a detrimental effect on the efficiency of the studied inhibitor under the experimental conditions adopted. For the tested inhibitor dosage, localized corrosion was found in 1Cr steel for all experimental conditions and on both microstructures.

The depth of the localized attack depends on the duration of pre-corrosion, but the tendency is opposite for both microstructures.

These results emphasize the importance of employing same the chemical composition and microstructure of steel to be used in service when performing inhibitor selection tests.

Acknowledgments

This work was supported by the Argentine Research Council for Science and Technology (CONICET), TENARIS and the Universidad Nacional de Mar del Plata.

References

[1] M.B. Kermani, L.M. Smith, CO_2 Corrosion Control in Oil and Gas Production. Design Considerations (EFC 23), Maney Publishing, London, 1997.
[2] S. Nesic, M. Nordsveen, R. Nyborg, A. Stangeland, Corrosion 59 (2003) 489.
[3] F.M. Song, Electrochim. Acta 55 (2010) 689.
[4] D.A. López, T. Perez, S.N. Simison, Mater. Des. 24 (2003) 561.
[5] M.B. Kermani, A. Morshed, Corrosion 59 (2003) 659.
[6] C. de Waard, U. Lotz, A. Dugstad, NACE Corrosion 95, Houston TX, USA, 1995 (Paper 128).
[7] A. Dugstad, H. Hemmer, M. Seiersten, NACE Corrosion 2000, Orlando, FL, USA, 2000 (Paper 24).
[8] P.I. Nice, H. Takabe, M. Ueda, NACE Corrosion 2000, Orlando, FL, USA, 2000 (Paper 154).
[9] M.B. Kermani, J.C. Gonzalez, G.L. Turconi, D. Edmonds, G. Dicken, L. Scoppio, NACE Corrosion 03, Houston, TX, USA, 2003 (Paper 116).
[10] M.B. Kermani, J.C. Gonzalez, G.L. Turconi, T. Perez, C. Morales, NACE Corrosion 04, Houston, TX, USA, 2004 (Paper 111).
[11] M.B. Kermani, J.C. Gonzales, G.L. Turconi, T. Pérez, C. Morales, NACE Corrosion 05, Houston, TX, USA, 2005 (Paper 111).
[12] M.B. Kermani, J.C. Gonzalez, C. Linne, M. Dougan, R. Cochrane, NACE Corrosion 01, Houston, TX, USA, 2001 (Paper 65).
[13] S.L. Fu, J.G. García, A. Griffin, NACE Corrosion 96, Houston, TX, USA, 1996 (Paper 21).
[14] S. Kapusta, S. Canter, NACE Corrosion 94, Houston, TX, USA, 1994 (Paper 10).
[15] T. Rogne, T.G. Eggen, U. Steinsmo, NACE Corrosion 96, Houston, TX, USA, 1996 (Paper 33).
[16] M.M. Salama, B.N. Brown, NACE Corrosion 09, Atlanta, GE, USA, 2009 (Paper 476).
[17] E. Gulbrandsen, S. Nesic, A. Stageland, T. Burchardt, S. Sundfaer, S.M. Hesjevik, S. Skjerve, NACE Corrosion 98, Houston, TX, USA, 1998 (Paper 13).
[18] E. Gulbrandsen, R. Nyborg, T. Loland, K. Nisancioglu, NACE Corrosion 2000, Orlando, FL, USA, 2000 (Paper 23).
[19] D.A. Lopez, W.H. Schreiner, S.R. de Sanchez, S.N. Simison, Appl. Surf. Sci. 207 (2003) 69.
[20] D.A. López, W.H. Schreiner, S.R. de Sanchez, S.N. Simison, Appl. Surf. Sci. 236 (2004) 77.
[21] D.A. López, S.N. Simison, S.R. de Sanchez, Electrochim. Acta 48 (2003) 845.
[22] D.A. López, S.N. Simison, S.R. de Sanchez, Corros. Sci. 47 (2005) 735.
[23] L.D. Paolinelli, T. Pérez, S.N. Simison, Corros. Sci. 50 (2008) 2456.
[24] J.L. Mora-Mendoza, S. Turgoose, Corros. Sci. 44 (2002) 1223.
[25] S. Turgoose, J.W. Palmer, G.E. Dicken, Corrosion 2005, Houston, TX, USA, 2005 (Paper 5275).
[26] L. Paolinelli, T. Pérez, S.N. Simison, NACE Corrosion 2006, San Diego, CA, USA, 2006 (Paper 369).
[27] D.A. Jones, Principles and Prevention of Corrosion, Macmillan Publishing Company, 1991.
[28] C. Cao, Corros. Sci. 38 (1996) 2073.
[29] V.S. Sastri, Corrosion Inhibitors, Principles and Applications, 1st ed., John Wiley & Sons Ltd., Chichester, 1998.
[30] G. Bailey, M.E.D. Turner, Ind. Corros. (1986) 8.
[31] J.L. Crolet, N. Thevenot, S. Nesic, Corrosion 54 (1998) 194.
[32] C.A. Palacios, J.R. Shadley, Corrosion 47 (1991) 122.
[33] M. Ueda, H. Takabe, NACE Corrosion 99, Houston, TX, USA, 1999 (Paper 13).
[34] K. Nose, T. Ishitsuka, H. Asahi, H. Tamehiro, Effects of Chromium Contents of Low-alloyed Steel and of Dissolved Oxygen in Aqueous Solution on Carbon Dioxide Corrosion (9), Advances in Corrosion Control and Materials in Oil and Gas Production (EFC 26), Maney Publishing, London, 1999.
[35] C.F. Chen, M.X. Lu, D.B. Sun, Z.H. Zhang, W. Chang, Corrosion 61 (2005) 594.